GSA Data Repository 2017359

Manzini et al., 2017, Weekly to monthly time scale of melt inclusion entrapment prior to eruption recorded by phosphorus distribution in olivine from mid-ocean ridges: Geology, doi:10.1130/G39463.1.

Supplementary data

Methodology

Sample preparation

Polished olivine grains with melt inclusions exposed at the surface were pressed into 1-inch indium mounts. Different glasses and San Carlos olivine were added to the sample mount to be used as reference material for P content determination by SIMS (see below).

To ensure that the melt inclusions were totally glassy, we acquired SEM images with a Tescan Mira LMU scanning electron microscope at the University of Lausanne.

Electron microprobe

All samples were analyzed by a JEOL 8200 Superprobe at the University of Lausanne. Analytical conditions for major element measurements in olivine were 15kV acceleration voltage, 20nA beam current and 5 μm beam size. Counting time was 30 sec for Si, Mg, Mn, Al and Fe and 40 sec for Ca, Ni and Cr. Natural minerals and synthetic oxides were used as standards. Analytical conditions for major element analyses in melt inclusions were 15kV, 10nA and 10 μm. Counting time was 30 sec on all elements, except for K (20 sec) and Na (16 sec). A glass standard (KL2-G) was used for SiO_2, Al_2O_3. Other elements were calibrated on specific minerals (e.g., a fayalite for Fe). ML3B-G was used as internal standard to check the calibration. Post-entrapment modification due to olivine crystallization (PEC% (% olivine

added), Table DR1) at the wall of melt inclusion was corrected for using the Petrolog software (Danyushevsky et al., 2000, 2002; Danyushevsky and Plechov, 2011).

X-rays distribution maps of melt inclusions and olivines were acquired by electron microprobe using a JEOL 8200 Superprobe at University of Lausanne. Analytical conditions were 15 kV, 10 nA, 0-1 μm probe diameter and 100 ms dwell-time with a 1-2 μm pixel size for major elements and 15kV, 200-250nA, 0-1 μm probe diameter and 100-230 ms dwell-time with a 1 μm pixel size for P, Al, Ni and Ca. X-ray elemental maps display higher count rate for P in MI compared to P-zoned olivine, as a result of the overlapping of the Ca (Kβ) second order peak with the P (Kα) peak. As olivine contains much less Ca than glass, the interference is negligible in olivine but not in MI. In any case, as olivine is homogeneous in Ca (Figure DR2), the structure on the phosphorus maps and profiles are only caused by variable P concentrations.

Secondary ion mass spectrometer

P concentrations in olivines and melt inclusions were analysed using a Cameca 1280-HR SIMS at the SwissSIMS laboratory (Lausanne, Switzerland). San Carlos (P = 40 ppm; Welsch et al., 2014) was used as standard for the olivine and BHVO-2G, BCR-2G, BIR-1G (P concentrations are from the certified values furnished by USGS) for the melt inclusions. Samples were sputtered with a 10 kV $^{133}Cs^{+}$ primary beam of 1 nA. Electron gun was used to compensate sample charge. A 15μm raster was used during pre-sputtering (90 sec) and analyses. Counting time was 0.48 on 29.9 (background), 1.04 s on ^{30}Si and 2.96 sec on ^{31}P. Waiting time was 0.8 s between each mass. Total time for each analysis was <6 min, including automatic centering of the secondary beam.^{30}Si and ^{31}P were detected on an axial electron multiplier. Entrance slit was set to 60 μm and exit slit to 200 μm, resulting in ~6000 mass resolving power. Field aperture was closed to 4000 μm. Energy slit was 50 eV.

Uncertainty on each point measurement (internal error) was < 5% (2σ %, average uncertainty of 0.95% 2σ) for P in olivine and <0.8% (2σ %, average uncertainty of 0.2% 2σ) in melt inclusion. The difference in reproducibility is due to counting statistic, melt inclusions having 100 times more counts on P. Reproducibility on the standard was < 4.5% (2SD) on the San Carlos and <1% (2SD) on BCR-2G.

Nanoscale secondary ion mass spectrometer

Profiles in olivines were obtained using the NanoSIMS at the Center of Advanced Surface Analysis (CASA, Lausanne, Switzerland). A Cs^+ primary beam was used to sputter olivine and the ion species $^{16}O^-$, $^{28}Si^-$, $^{31}P^-$, $^{24}Mg^{16}O^-$, $^{27}Al^{16}O^-$ and $^{31}P^{16}O^-$ were extracted and measured using electron multipliers. In order to prevent the build-up of a charge on the sample's surface, the surfaces were coated with a 10-15nm gold layer. MRP was > 8000 and no peak overlap was observed.

After identification of the area of interest using the CCD camera of the NanoSIMS, a 25 x 25 µm image of the area of interest was first acquired (with a 256 x 256 pixel resolution corresponding to a pixel size ~100 nm). Using the NanoSIMS software, the locations of the linescan were precisely selected to be perpendicular to the transition identified by EMPA analyses. The line scans were acquired using a two-step approach. First a pre-sputtering phase was performed for 2 cycles with a dwell time of 2sec/pixel, using slightly larger beam size to clean up the surface (diaphragm D1-2, and 3.8pA for the Cs^+ primary beam). The acquisition of the high resolution line scans were performed using a finer beam (D1-3, ~150nm, and 1.7pA for the Cs+ beam) over 5 cycles with 2sec/pixel. $^{24}Mg^{16}O^-$ data were used to monitor possible local variation in the ionization and extraction processes as it is expected to be homogeneous in the olivine measured. ^{16}O, ^{18}O, ^{24}Mg, ^{27}Al, ^{28}Si, ^{31}P and $^{31}P^{16}O$ were acquired at the same time. In order to minimize the instrumental drift, we normalized the profiles to ^{28}Si, which is, based on EMPA X-ray maps, homogeneous within the olivine and

the MI. The NanoSIMS session was not standardized, resulting in a ^{31}P count rate higher in the MI than in P-zoned olivine, due to matrix effects.

Diffusion Chronometry and Fit of Diffusion Profiles

The 2D profiles were measured perpendicular to the zonation. The following parameters were assumed for the diffusion calculations and fitting of the profiles: 1- each P-enriched band was homogeneous at the beginning or represents a line source; 2- the contact between the P-rich and P-poor zones was a step function. Thin, linear features with no plateau were modelled as a line source, while P-enriched zones displaying a plateau were modeled as step functions. Specifically, a P-peak of a few μm width (e.g. Fig. 2) was modelled as line source, while b) P-enriched zones larger than 10 μm were modelled as individual step functions (e.g. Fig. DR5).

We used the diffusion coefficient for P diffusion in olivine reported by Watson et al. (2015) based on their diffusion experiments in olivine which are $\log(D_0,m^2/s) = -10.06 \pm 0.80$ and $E_a = 229 \pm 16$ kJ/mol. Error functions were fit to each of the measured profiles using a weighted Marquardt fitting routine (Press et al., 1992).

The uncertainty of the fit was estimated using the $\chi 2$ per point. The uncertainty, expressed as 2σ, for each point was estimated from the variation in the part of the profiles considered to be flat. Initial conditions of the model are the bigger source of uncertainty. Since the line source diffusion modeling assumes an infinite band width of P-enrichment, the calculated values are maximum time estimates.

MELTS calculations

MELTs version 5.0 was used. The principles of the program are summarised in Ghiorso and Sack (1995). We used the average composition of the individual melt inclusions and 0.15 wt% H_2O. We then determined the liquidus temperature, followed by decompression calculations slightly below the liquidus temperature. Isentropic, isenthalpic and isothermal decompression

calculations were done between 2 kbar and 0.1 kbar in steps of 0.1 kbar, with a fixed fO_2 (QFM -2).

Figures

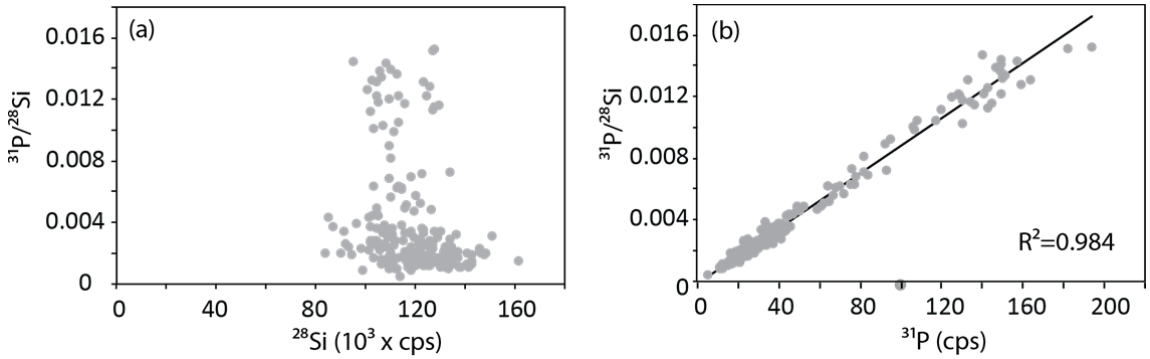

Figure DR1: Plot of $^{31}P/^{28}Si$ ratios obtained during NanoSIMS measurements versus (a) ^{48}Si counts and (b) ^{31}P counts. The absence of correlation in (a) and the good correlation in (b) indicates that $^{31}P/^{28}Si$ ratio depends on ^{31}P concentration only.

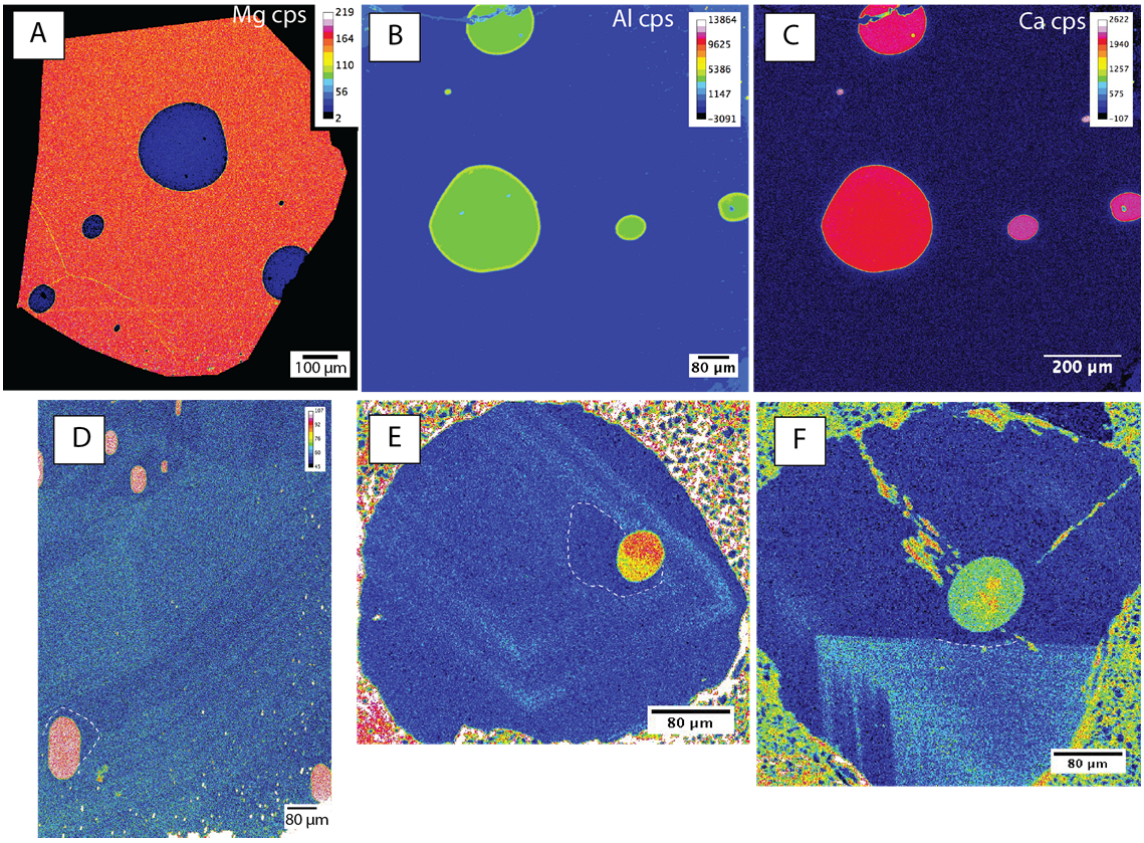

Figure DR2: X-ray maps for A- Mg concentration in ARP73-10-03_16; B- Al concentration in ARP73-10-03_16; C- Ca concentration in ARP73-10-03_16; D- P concentration in CH77-DR6-203_52; E- P concentration in CH77-DR6-203_4; F- P concentration in CH77-DR6-203_8. Note the homogeneity of the olivine in major elements (A, B and C), whereas nice P zonations are present in the same olivine (Figure 1). MI are homogeneous in P, except in Fig. DR2-E. Apparent heterogeneity of this specific MI is explained by the presence of a previous SIMS analysis spot, creating a small topography, able to slightly modify the P signal during P imaging by EMPA.

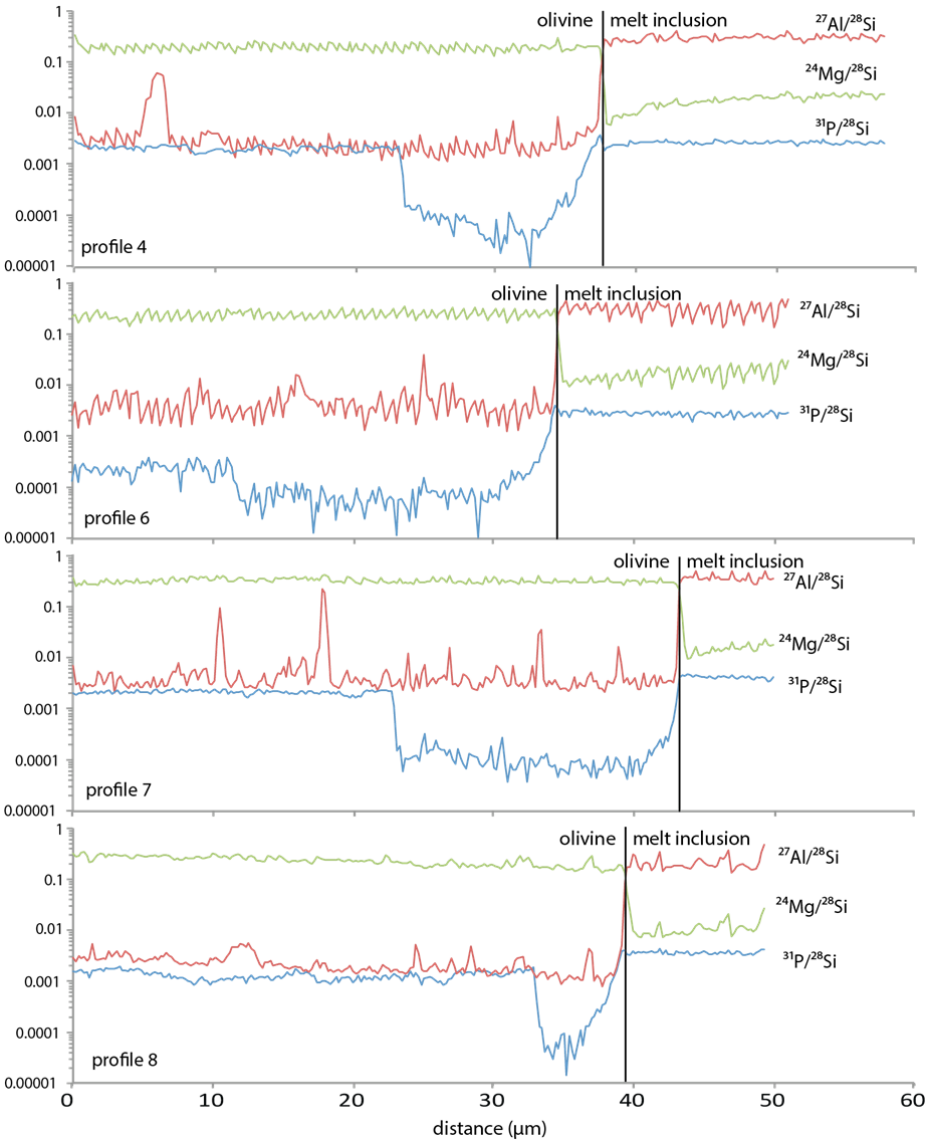

Figure DR3:

$^{31}P/^{28}Si$ profiles realized in the ARP73-10-03_16 olivine and melt inclusions for all the measured elements. The contact between MI and olivine can be determined based on the Mg and Al profiles. The location of the profiles is presented in Figure 1.

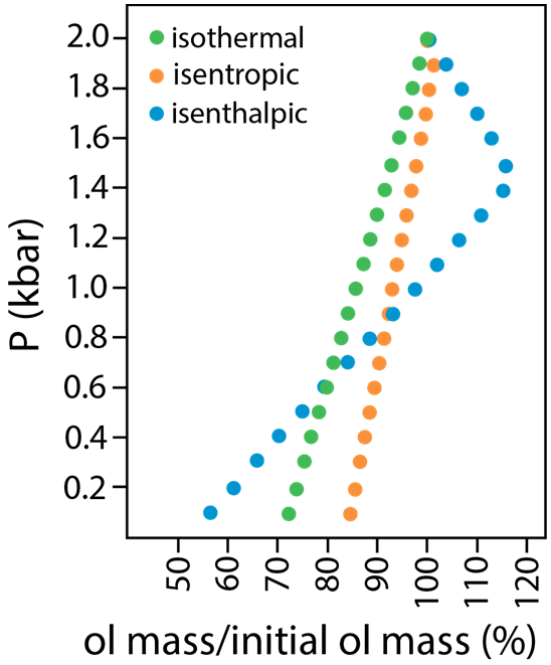

127

128 Figure DR4: Results of the MELTS decompression calculations at fixed fO_2 (QFM) between
129 2 to 0.1 kbar for isothermal, isenthalpic and isentropic decompression. Ol is for olivine.
130 Isentropic and isenthalpic decompression causes weak to moderate initial resorption, while
131 isothermal decompression only causes crystallization.

132

133

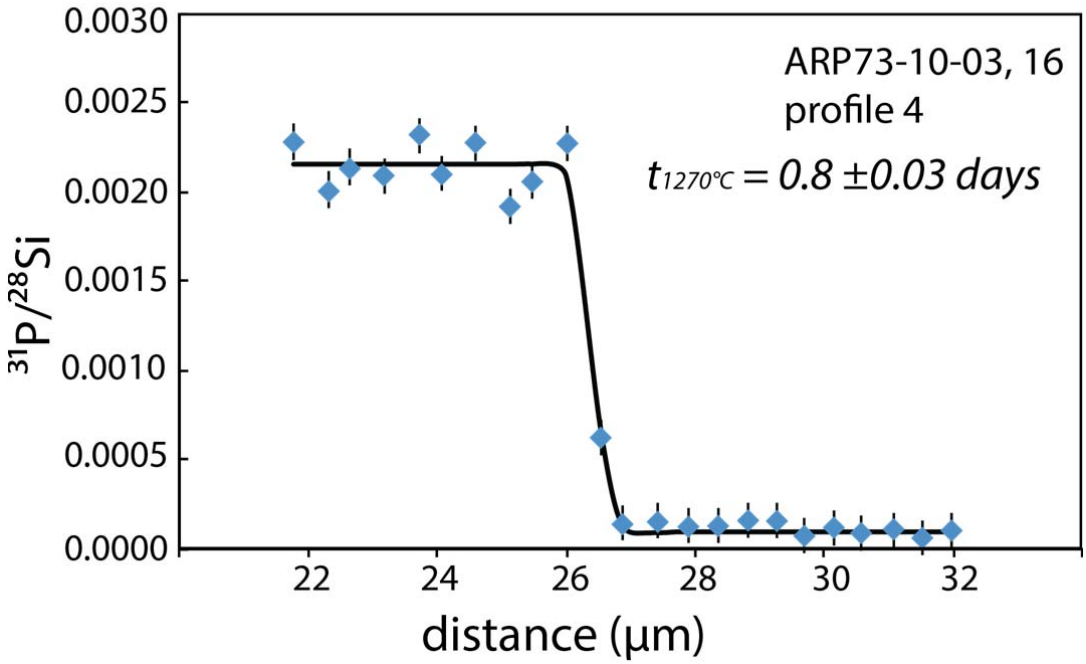

134

135 Figure DR5: Comparison of the measured $^{31}P/^{28}Si$ profile in olivine with the calculated curve
136 derived from semi-infinite source diffusion modeling for profile 9, at the contact between P-
137 rich olivine and P-depleted halo. Diffusion was 0.8 days at 1270°C, using D from Watson et
138 al. (2015). This estimated time scale is a maximum, since the profile is near vertical, and its
139 width is constraint by one point which could represent an analytical artefact. In fact, the
140 profile width could be significantly overestimated.

141

142 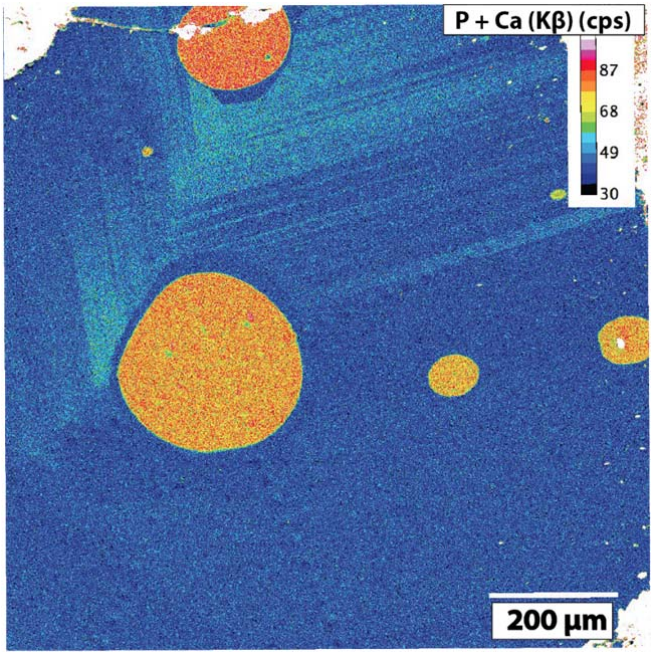

143 Figure DR6: P distribution in ARP73-10-03_16 olivine.

144

145 ## Tables

146 Table DR1

147 NanoSIMS measurements of the profile 9 realized in the ARP73-10-13_16 olivine.

148

Table DR1

Distance (um)	31P (cps)	28Si (cps)
18.0858400	19	97678
18.3477400	26	121670
18.5226800	11	111065
18.7845900	18	126832
18.9595300	18	108121
19.2214400	24	125457
19.3963800	23	105542
19.6582900	34	142189
19.8332200	41	147602
20.0951400	37	145394
20.2700700	37	111402
20.5319900	46	127164
20.7069200	44	102883
20.9688400	72	126160
21.1437600	82	100907
21.4056900	136	117867
21.5806100	92	101973
21.8425400	159	124376
22.0174600	148	106587
22.2793900	149	122282
22.4543000	133	101183
22.7162500	182	119846
22.8911500	157	109615
23.1531000	194	127241
23.3280000	149	108946
23.5899500	145	125116
23.7648500	147	105254
24.0268000	164	124435
24.2017000	125	104253
24.4636500	143	126520
24.6385400	107	108187
24.9005000	93	127452
25.0753900	70	112467
25.3373500	42	129259
25.5122400	33	109530
25.7742000	42	122799
25.9490900	32	109173
26.2110500	42	126676
26.3859400	20	111107

Distance (um)	31P (cps)	28Si (cps)
26.6479000	20	133279
26.8227900	21	112554
27.0847500	27	135998
27.2596300	24	119142
27.5216000	33	127031
27.6964800	32	133735
27.8716300	27	115507
28.1333300	23	123117
28.3084800	16	108431
28.5701800	26	124510
28.7453200	17	109618
29.0070300	20	133930
29.1821600	14	126906
29.4438800	23	134133
29.6190000	27	145317
29.8807300	25	147300
30.0558500	25	115786
30.3175800	23	136501
30.4926900	16	126328
30.7544300	24	129967
30.9295300	18	117576
31.1912700	15	135174
31.3663800	18	116562
31.6281200	18	136904
31.8032200	23	121893
32.0649700	22	130770
32.2400700	15	118591
32.5018200	17	142127
32.6769100	15	120532
32.9386700	25	137011
33.1137600	19	121271
33.3755200	32	134642
33.5506000	22	120888
33.8123700	27	136803
33.9874500	20	119072
34.2492200	21	125619
34.4242900	12	106236
34.6860700	14	126237
34.8611400	12	110990

149 Table DR2

150 Major element compositions (determined by EPMA) and P concentration (determined by

151 SIMS) of the melt inclusions hosted in the ARP73-10-13_16 olivine. Values measured for

152 ML3B glass, used as external standard for EPMA glass analyses, are also reported. Major

153 element concentrations are given in wt% and P concentrations in ppm. For ML3B FeO

154 represents FeO_{tot}.

Table DR2

Sample	SiO2	TiO2	Al2O3	Fe2O3	FeO	MnO	MgO	CaO	Na2O	K2O	% ol added	P (ppm)	2sd%
ARP73_16a	49.52	0.59	14.42	0.91	7.83	0.12	12.07	12.96	1.51	0.07	10.9	374	0.07
ARP73_16b	49.81	0.53	14.44	0.88	7.58	0.09	11.68	13.41	1.51	0.08	12.7	495	0.06
ARP73_16c	49.71	0.55	14.53	0.87	7.63	0.14	11.80	13.28	1.43	0.06	17.0	297	0.09
ARP73_16d	48.97	0.59	14.85	0.90	7.77	0.12	11.83	13.33	1.57	0.07	17.3	311	0.08
ML3B	51.56	2.10	13.72	n.d.	11.59	0.17	6.59	10.33	2.52	0.39		n.d.	

156 Table DR3

157 Results of the MELTs calculations for the three different models tested.

Table DR3

isothermal decompression				isentropic decompression				isenthalpic decompression			
T (C)	P (kbars)	mass (mg)	forsterite	T (C)	P (kbars)	mass (mg)	forsterite	T (C)	P (kbars)	mass (mg)	forsterite
1240	2	5.194	84.27	1250	2	4.1818	84.70	1230	2	5.2288	83.59
1240	1.9	5.1211	84.30	1248.7	1.9	4.242	84.67	1229.6	1.9	5.3998	83.65
1240	1.8	5.0479	84.33	1248.3	1.8	4.2044	84.69	1229.1	1.8	5.5621	83.71
1240	1.7	4.9744	84.36	1248	1.7	4.1666	84.71	1228.6	1.7	5.7184	83.76
1240	1.6	4.9005	84.40	1247.6	1.6	4.1286	84.72	1228.1	1.6	5.8691	83.82
1240	1.5	4.8262	84.43	1247.2	1.5	4.0904	84.74	1227.6	1.5	6.0147	83.87
1240	1.4	4.7516	84.46	1246.9	1.4	4.0521	84.76	1227.6	1.4	5.9872	83.92
1240	1.3	4.6767	84.50	1246.5	1.3	4.0135	84.77	1229.2	1.3	5.7603	84.02
1240	1.2	4.6014	84.53	1246.1	1.2	3.9748	84.79	1230.7	1.2	5.5322	84.12
1240	1.1	4.5258	84.56	1245.8	1.1	3.936	84.81	1232.3	1.1	5.303	84.23
1240	1	4.4498	84.60	1245.4	1	3.8969	84.83	1233.8	1	5.0728	84.33
1240	0.9	4.3735	84.63	1245	0.9	3.8577	84.84	1235.4	0.9	4.8414	84.43
1240	0.8	4.2968	84.66	1244.6	0.8	3.8182	84.86	1236.9	0.8	4.6089	84.53
1240	0.7	4.2197	84.70	1244.3	0.7	3.7787	84.88	1238.5	0.7	4.3753	84.63
1240	0.6	4.1423	84.73	1243.9	0.6	3.7389	84.90	1240	0.6	4.1406	84.73
1240	0.5	4.0645	84.77	1243.5	0.5	3.6989	84.92	1241.6	0.5	3.9048	84.83
1240	0.4	3.9864	84.80	1243.2	0.4	3.6588	84.94	1243.1	0.4	3.6678	84.93
1240	0.3	3.9079	84.83	1242.8	0.3	3.6185	84.95	1244.6	0.3	3.4297	85.03
1240	0.2	3.829	84.87	1242.4	0.2	3.578	84.97	1246.1	0.2	3.1905	85.13
1240	0.1	3.7497	84.90	1242	0.1	3.5373	84.99	1247.6	0.1	2.9501	85.23

References

Crank, J., 1975. The mathematics of diffusion, Oxford University Press. doi:10.1016/0306-4549(77)90072-X

Danyushevsky, L. V., Plechov, P., 2011. Petrolog3: Integrated software for modeling crystallization processes. Geochemistry, Geophys. Geosystems 12. doi:10.1029/2011GC003516

Danyushevsky, L. V, Della, F.N., Sokolov, S., 2000. Re-equilibration of melt inclusions trapped by magnesian olivine phenocrysts from subduction-related magmas : petrological implications. Contrib. to Mineral. Petrol. 138, 68–83.

Danyushevsky, L. V, Sokolov, S., Falloon, T.J., 2002. Melt Inclusions in Olivine Phenocrysts : Using Diffusive Re-equilibration to Determine the Cooling History of a Crystal , with Implications for the Origin of Olivine-phyric Volcanic Rocks. J. Petrol. 43, 1651–1671. doi:10.1093/petrology/43.9.1651

Ghiorso, M.S., Sack, R.O., 1995. Chemical mass transfer in magmatic processes IV . A revised and internally consistent thermodynamic model for the interpolation and extrapolation of liquid-solid equilibria in magmatic systems at elevated temperatures and pressures. Contrib. to Mineral. Petrol. 119, 197–212.

Press, W.H., Flannery, B.P., Teukolsky, S.A., Vetterling, A. t., 1992. Numerical Recipes in C: The Art of Scientific Computing. New York, cambrige Univ. Press 2nd ed, 994 p.

Watson, E.B., Cherniak, D.J., Holycross, M.E., 2015. Diffusion of phosphorus in olivine and molten basalt. Am. Mineral. 100, 2053–2065. doi:10.2138/am-2015-5416

Welsch, B., Hammer, J., Hellebrand, E., 2014. Phosphorus zoning reveals dendritic architecture of olivine. Geology 42, 867–870. doi:10.1130/G35691.1